2024 IEEE/RSJ International Conference on Intelligent Robots and Systems (IROS)
October 14-18, 2024. Abu Dhabi, UAE

PARE: A Plane-Assisted Autonomous Robot Exploration Framework in Unknown and Uneven Terrain

Pu Xu, Zhaoqiang Bai, Haoming Liu, and Zheng Fang*

***Abstract*— Identifying traversable areas is a critical task for unmanned vehicles exploring safely through unstructured environments. In practice, the ambiguity in perceiving terrain traversability usually brings great challenges for autonomous exploration in unknown and uneven terrain, which often leads to conservative strategies or potential risk of vehicle damage, resulting in many unexplored areas in the environment. To that end, this paper proposes a plane-assisted autonomous robot exploration framework (PARE) to achieve maximum volume and safe autonomous exploration. The process is carried out by a three-step dual-layer framework: constructing a local tree using Plane-Assisted RRT* (PA-RRT*), calculating exploration gain based on terrain information, and maintaining a global search graph. Firstly, the planar feature metrics (flatness, sparsity, elevation variation, slope and slope variation) are introduced to determine the terrain traversability. Secondly, to completely explore the rugged environment, we propose a dual-layer exploration framework comprising local and global strategies. A local planner based on PA-RRT* is proposed to find the best path by evaluating the planar information and the volumetric gain within the local exploration tree. Meanwhile, a global planner constructed by graph is proposed to record unexplored nodes with high exploration gain from the local tree to ensure a high level of exploration volume. Extensive simulation and real-world experiments demonstrate that our method significantly outperforms existing frameworks, with an average improvement of more than 12% in exploration volume.**

I. INTRODUCTION

Autonomous exploration stands as an indispensable technology, empowering unmanned ground vehicles (UGV) with the capability to effectively and securely construct environment models in predefined unknown areas. This technology finds wide-range applications in industrial inspection [1], object search [2], and scene reconstruction [3]. Despite the numerous successes of autonomous exploration in structured environments, unfortunately, challenges emerge when deploying autonomous exploration vehicles in large-scale and intricate outdoor scenarios, such as rugged mountains [4] or dense forestry [5]. The existing methods [6]–[8], which are tailored for flat terrain, struggle to cope with the complexities posed by challenging and hazardous terrain such as steep slopes and hollows, as illustrated in Fig. 1. The complex terrain may cause ambiguity regarding the traversability of the area, potentially heightening the chances of UGV rolling over or misjudging traversable regions.

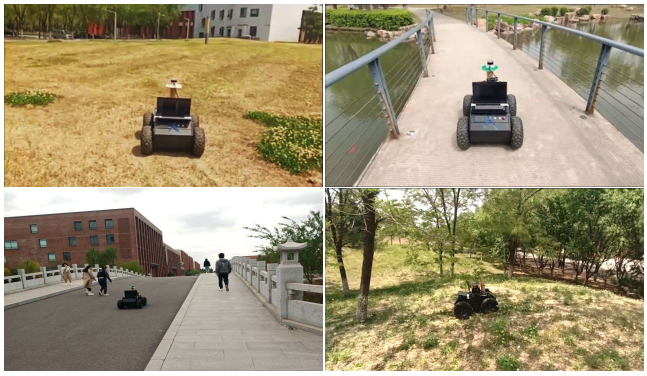

Fig. 1. The Bulldog, a four-wheel differential mobile platform, serves as the primary experimental vehicle to validate the robust exploration capabilities of PARE in various challenging terrains. Our experiments are strategically conducted across various environments, including steep slopes, flat bridges, dense forests, and arch bridges.

Therefore, the primary challenges addressed in this paper are how to assess the uneven terrain to identify traversable paths and how to maximize the exploration volume in unknown and uneven environments. The main objective is to optimize the exploration volume in unpredictable and unstructured areas while ensuring UGV navigates safely through challenging terrain and reducing the potential of accidents and incorrect assessment.

To achieve this goal, this paper proposes **PARE** (**P**lane-Assisted **A**utonomous **R**obot **E**xploration), a hierarchical framework designed to facilitate robots exploring autonomously and safely in unknown and uneven terrain. *Firstly*, considering the inherent dangers presented in such environments and the fact that UGV primarily focuses on the planar information, we introduce planar feature metrics, including flatness, sparsity, elevation variation, slope and slope variation, to evaluate the traversability cost of the plane fitted by sampling points of Rapidly-exploring Random Trees (RRT). *Secondly*, due to the significant elevation variations in rugged hills terrain and the existence of numerous subpaths, UGV encounters challenges in determining the optimal exploration path. This paper employs a dual-layer exploration framework that integrates local and global exploration strategies. We present a local planner PA-RRT* (a variant of RRT) that constructs a local exploration tree to store planar information and compute exploration gain including

This work was supported in part by the National Natural Science Foundation of China under Grant 62073066, in part by the Fundamental Research Funds for the Central Universities under Grant N2226001, and in part by 111 Project under Grant B16009. (Corresponding author: Zheng Fang.)

The authors are all with the Faculty of Robot Science and Engineering, Northeastern University, Shenyang 110819, China (e-mail: {2210748@stu, 2100711@stu, 2302151@stu, fangzheng@mail}.neu.edu.cn). Zheng Fang is also with the National Frontiers Science Center for Industrial Intelligence and Systems Optimization, and also with the Key Laboratory of Data Analytics and Optimization for Smart Industry, Ministry of Education, Northeastern University, Shenyang 110819, China.

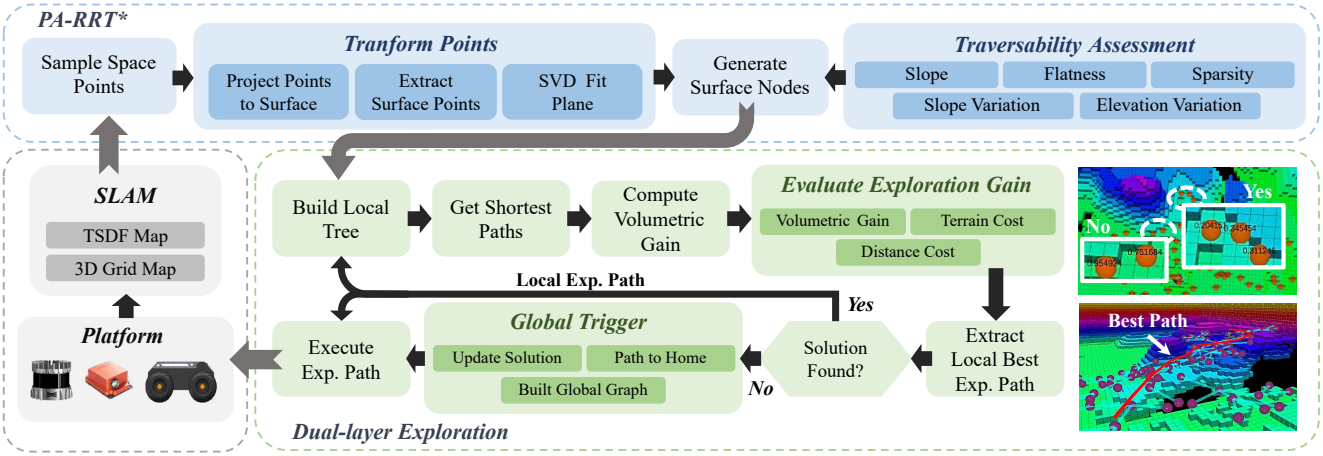

Fig. 2. Architecture of the proposed framework. The onboard computer processes real-time point clouds and odometry from LiDAR and SLAM. Then, the SLAM module updates the TSDF map and 3D grid map. After acquiring valid sampling space points extracted from map updates, surface nodes are generated based on transform points and traversability assessment within PA-RRT*. The dual-layer exploration framework constructs a local exploration tree and maintains a global exploration graph. Through the evaluation of exploration gain in branches, PARE determines the best exploration path for UGV within the framework. (Exp. indicates Exploration)

volumetric gain, terrain cost and distance cost. The best local path is chosen by acquiring the higher exploration gain while ensuring minimal terrain cost. A global search graph is also proposed to store the starting node and unexplored nodes with the high exploration gain from the local tree. This ensures a high level of exploration volume, thereby enabling the ground robot to traverse through rugged terrain more efficiently along a rational exploration route. *Finally*, we conduct experiments in simulation and real-world scenes to demonstrate the capability of maximum volume and safe exploration of our proposed method in uneven terrain. The main contributions of this paper are summarized as follows:

- A new sampling-based algorithm named PA-RRT* is proposed for ensuring safe exploration in uneven terrain, which utilizes five planar feature metrics to determine traversable areas.
- A novel dual-layer plane-assisted autonomous robot exploration framework (PARE) is proposed, which enables the robot to obtain a larger exploration volume in uneven terrain by combining local and global strategies.
- Extensive simulation and real-world experiments demonstrate the advantages and robustness of our proposed method, especially the capability of supporting maximum volume and safe exploration of ground vehicles in challenging and uneven scenarios.

II. RELATED WORK

A. Terrain Assessment for Navigation

The assessment of terrain characteristics plays a key role in impacting the capability of the robot to explore uneven terrain. Therefore, to achieve safe and efficient exploration in such environments, it is imperative to assess the comprehensive terrain information. Some methods require explicit construction of maps to determine traversable areas indirectly. While probability occupancy maps [9] can effectively handle perceptual uncertainty of the terrain, challenges arise with false detection and escalating memory requirements as the state space dimension expands. An alternative approach involves elevation maps [10], known for its computational efficiency and storage-friendly properties. However, elevation maps exhibit large deviations in grid height values, potentially missing crucial terrain information. Other methods directly apply point clouds to determine feasible areas. In rugged terrain, 3D terrain reconstruction becomes essential to create a comprehensive 3D geometric model, using structures such as 3D mesh grid [11] or polygon mesh [12]. Although [13] directly infer local terrain surfaces from unordered point clouds without reconstruction, the planning safety heavily relies on the density of point clouds. For scenarios demanding better precision, the RGBD camera is more commonly employed [14]. PUTN [15] employs a custom terrain assessment and fits planes on point clouds to generate a sparse path, alleviating the computational burden associated with constructing and maintaining a topographic map. However, it lacks adaptability to extreme or highly irregular terrain, which leads to inaccuracies in path planning. The terrain evaluation method proposed in this paper draws inspiration from [15]. We propose different planar feature metrics to enable robots to generate safe paths and adapt to varying terrain conditions, thereby enhancing the application potential of robots across challenging environments.

B. Autonomous Exploration

Autonomous exploration in robotics is primarily addressed by two solutions: frontier-based [16]–[19] and sampling-based [20]–[23] approaches. Frontier-based methods focus on identifying the boundary between known and unknown spaces for exploration targets, but they can sometimes exhibit excessive aggressiveness, leading to suboptimal efficiency. On the other hand, sampling-based methods randomly select viewpoints and then determine the optimal ones using a cost function to observe more unknown areas, but this method involves extensive calculations and lacks global

guidance. In response to the challenges posed by large-scale and complex environments, several recent approaches have combined ideas from both frontier-based and sampling-based methods [7], [8], [24]–[26], which employ a dual-layer exploration framework encompassing both local and global exploration. When the local exploration tree yields minimal gains compared to the branches out in the global exploration tree, the planner switches to the global exploration graph to extend the exploration. GBP [24] specifically focuses on two rapidly-exploring random graphs (RRG) with different densities serving as local and global planners. While it ultimately selects edges from the RRG as the exploration path, this approach may result in suboptimal solutions during global exploration. TARE [8] explores unknown space by traversing viewpoints along the shortest path, but its computation is time-consuming and it fails to consider exploration gain, potentially leading to increased exploration time and traveling distances. FAEL [27] improves TARE by introducing rapid preprocessing for environmental information and optimizing the exploration path to facilitate the exploration process. However, these methods often ignore uneven and rugged terrain, neglecting possible traversable areas and posing dangers for robots during exploration. In contrast, we propose a novel dual-layer exploration framework that incorporates a planar assessment to overcome the shortcomings of existing exploration algorithms, which ensures an accurate analysis of traversable regions and promotes efficient exploration.

III. METHODOLOGY

A. Problem Formulation

The proposed framework, as depicted in Fig. 2, tackles the challenges of autonomous exploration faced by ground robots in complex terrain, including rugged hills and deep hollows that impose significant traversability constraints. Due to the absence of comprehensive terrain information in wild environments and the existence of numerous sub-paths, the robot encounters difficulty in deducing the optimal exploration path. Hence, a dual-layer exploration framework is introduced by combining local and global strategies. Let $\mathcal{M}$ denote a 3D occupancy map of the space, which is incrementally constructed over time. The subset $\mathcal{M}_{sub} \subset \mathcal{M}$ represents the presently explored local map. Considering a volume $\mathcal{V}$ within the specified space, the volume of the explored space is denoted as $\mathcal{V}_{exp}$. In uncertain and rugged terrain, where the residual area $\mathcal{V}_{res} = \mathcal{V} \backslash \mathcal{V}_{exp}$ cannot be accurately determined, this paper sets that the robot should return to its starting position when sub-branches in global exploration have been thoroughly explored or when the ratio $\mathcal{V}_{exp}/\mathcal{V}$ reaches 95%. The local planner explores each $\mathcal{M}_{sub}$ through an iterative process while considering diverse terrain features around the robot. It generates a safe and traversable path within the local map $\mathcal{M}_{sub}$, which guides the robot to explore the unknown space $\mathcal{M}_{unkonwn} \subset \mathcal{M}$. The traversable path conforms to the following criteria: (1) ensuring complete traversability; (2) avoiding the risk of the robot rolling over, and (3) finding a balance between terrain risk and maximum exploration volume. After completing the local exploration, the global planner determines the global path for either continuing exploration or returning to the starting position. The global path also adheres to the same criteria as the local paths mentioned above.

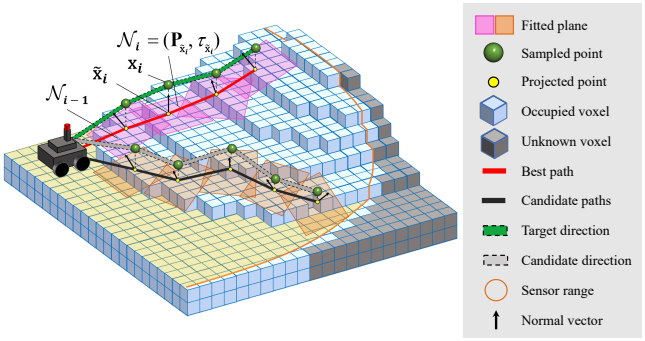

Fig. 3. Representation of exploration path generation in complex terrain. The planner path is defined as a sequence of nodes $\{\mathcal{N}_0, \mathcal{N}_1, ..., \mathcal{N}_n\}$ extended by the sampling tree. Each node $\mathcal{N}_i$ consists of a 6D pose $\mathbf{P}_{\tilde{\mathbf{x}}_i}$ and a traversability $\tau_{\tilde{\mathbf{x}}_i}$.The orange and pink rectangles indicate a sequence of planes $\{P_i\}$ fitted by surface points $\{\tilde{\mathbf{x}}_i\}$. The red and black lines respectively represent the best path and candidate paths.

B. Plane-Assisted RRT*

1) 3D Representation and Terrain Assessment:

The efficiency of exploration in uneven terrain is influenced by the representation of the environment. Let us define $\mathcal{X} \in \mathbb{R}^3$ as the configuration space. Let $\mathcal{X}_{surf} \in \mathcal{X}$ represent the areas near the ground, $\mathcal{X}_{obs} \in \mathcal{X}$ denote the occupied space, and $\mathcal{X}_{free} = \mathcal{X} \backslash \mathcal{X}_{obs}$ signify the free space. To specifically define the region traversable by ground robots, we introduce $\mathcal{X}_{trav}$ as the subset of $\mathcal{X}_{free} \cap \mathcal{X}_{surf}$. Consider a point $\mathbf{x}_i \in \mathbb{R}^3$, and denote the projection onto the terrain surface as $\tilde{\mathbf{x}}_i = [x, y, \bar{z}]^T$. Here, $\bar{z} = \min\{z - k \cdot res/2 \mid \tilde{\mathbf{x}}_i \in \mathcal{X}_{obs}, \bar{z} \geq z_l, k \in \mathbb{N}\}$, where z_l indicates the predefined threshold of minimum elevation and res is the grid map resolution. The terrain assessment process begins with the transform points module, which firstly projects a space point $\mathbf{x}_i$ to obtain a surface point $\tilde{\mathbf{x}}_i$. Then, the SVD method is employed to fit a plane P_i based on a point cloud within a cube centered at $\tilde{\mathbf{x}}_i$ with a constant side length l_{cube}, which is represented as $\Omega_i = \{(\tilde{\mathbf{x}}_i)_{j=1:N_i}\}$. As depicted in Fig. 3, each plane is then represented as a node $\mathcal{N}_i = (\mathbf{P}_{\tilde{\mathbf{x}}_i}, \tau_{\tilde{\mathbf{x}}_i})$, where $\mathbf{P}_{\tilde{\mathbf{x}}_i}$ signifies the 6D pose of the robot and τ_i indicates the traversability of the plane. Here, $\tau_{\tilde{\mathbf{x}}_i} \in [0, 1]$, where 1 indicates the terrain is absolutely unsuitable to be traversable, and 0 means the terrain is completely traversable.

Analyzing the terrain costs of nodes is crucial for path planning in rugged terrain. It allows for the identification and elimination of nodes that bring higher risks of collisions or difficulties in traversable areas. We propose a planar assessment method with five feature metrics: slope s, slope variation $\Delta s_{i,i+1}$, elevation variation $\Delta e_{i,i+1}$, flatness f, and sparsity λ for terrain assessment. Slope s encourages the selection of terrain with gentle slopes; $\Delta s_{i,i+1}$ and $\Delta e_{i,i+1}$ denote the differences in slope and elevation between the planes of two nodes, correspondingly. $\Delta s_{i,i+1}$ imposes stricter penalties on terrain with frequent fluctuations,

Algorithm 1: Plane-Assisted Local Planner

Input : Vertex Set $\mathbb{V}$; Edge Set $\mathbb{E}$; Local Tree $\mathbb{T}_L$; Current state ψ_c

Output: Best path $\sigma_{L,\,best}$

$\psi_c \leftarrow$ **GetCurrentConfiguration**();
for $i = 1$ **to** k **do**
  $\mathbb{V} \leftarrow \{\psi_c\}; \mathbb{E} \leftarrow \emptyset; \mathbb{T}_L = (\mathbb{V}, \mathbb{E})$;
  $\mathbf{x}_{rand} \leftarrow$ **SampleSpacePoint**();
  $\tilde{\mathbf{x}}_{rand} \leftarrow$ **ProjectToSurface** $(\mathbf{x}_{rand})$;
  $\tilde{\mathbf{x}}_{near} \leftarrow$ **NearestVertex** $(\mathbb{T}_L, \tilde{\mathbf{x}}_{rand})$;
  $\tilde{\mathbf{x}}_{new} \leftarrow$ **Steer** $(\tilde{\mathbf{x}}_{rand}, \tilde{\mathbf{x}}_{near}, l_{cube}/2)$;
  $\mathcal{N}_{new}\,(\mathbf{P}_{new}, \tau_{new}) \leftarrow$ **FitPlane** $(\tilde{\mathbf{x}}_{new})$;
  $\mathcal{F}(\mathcal{N}_{new}, \mathcal{N}_{near}) \leftarrow$ **TerrainCost** $(\tilde{\mathbf{x}}_{new}, \tilde{\mathbf{x}}_{near})$;
  if $P_{new} \in \mathcal{X}_{trav}$ ***and*** $\Delta e_{new,near} < \Delta e_{max}$ **then**
    $\Xi_{neighbor} \leftarrow$ **FindNeighbors** $(\mathbb{T}_L, \mathcal{N}_{new})$;
    while $\Xi_{neighbor} \neq \emptyset$ **do**
      $\mathcal{N}_{parent} \leftarrow$ **GetParent** $(\Xi_{neighbor}, \mathcal{N}_{new})$;
      if $\mathcal{F}(\mathcal{N}_{new}, \mathcal{N}_{parent}) < \mathcal{F}(\mathcal{N}_{new}, \mathcal{N}_{near})$ **then**
        $\mathbb{T}_L \leftarrow \mathbb{V} \cup \{\mathcal{N}_{new}\}, \mathbb{E} \cup \{\mathcal{N}_{new}, \mathcal{N}_{parent}\}$;
        $\mathbb{T}_L \leftarrow$ **Rewire** $(\mathbb{T}_L, \Xi_{neighbor}, \mathcal{N}_{new})$;
      end
    end
  end
end
$\Sigma_{\sigma,L} \leftarrow$ **GetShortestPaths**$(\mathbb{T}_L, \psi_c)$;
ComputeVolumetricGain$(\mathbb{T}_L)$;
$\Sigma_{E(\sigma_L)} \leftarrow$ **EvaluateExplorationGain** $(\mathbb{T}_L, \Sigma_{\sigma,L})$;
$\sigma_{L,best} \leftarrow$ **FindBestPath** $\left(\Sigma_{E(\sigma_L)}\right)$;
return $\sigma_{L,best}$

while $\Delta e_{i,i+1}$ discourages choosing planes with significant difference in elevation. Flatness f prioritizes flat terrain for robot movement to minimize energy consumption. Sparsity λ encourages avoiding unknown ground and hazardous terrain. The terrain cost of the path between two nodes is defined as follows:

$$\mathcal{F}\left(\mathcal{N}_i, \mathcal{N}_{i+1}\right) = \omega_1 \left(\frac{1}{1-\tau_{\tilde{\mathbf{x}}_i}} + \frac{1}{1-\tau_{\tilde{\mathbf{x}}_{i+1}}} - 2 \right) + \omega_2 \frac{1}{\Delta s_{\max} - \Delta s_{i,i+1}} + \omega_3 \frac{1}{\Delta e_{\max} - \Delta e_{i,i+1}} \tag{1}$$

$$\tau_{\tilde{\mathbf{x}}_i} = \alpha_1 \frac{s}{s_{\max}} + \alpha_2 \frac{f}{f_{\max}} + \alpha_3 \frac{\lambda}{\lambda_{\max}} \tag{2}$$

where ω_1, ω_2, ω_3 are the penalty scale factors. The weights α_1, α_2, and α_3 sum up to 1. $s_{\max}$, $\Delta s_{\max}$, $\Delta e_{\max}$, $f_{\max}$, $\lambda_{\max}$ represent the maximum value for each evaluation indicator. The above five indicators are defined as follows:

$$s = \kappa_s \arcsin \bar{z}_{e^z} \tag{3}$$

$$\Delta s_{i,i+1} = s_i - s_{i+1} \tag{4}$$

$$\Delta e_{i,i+1} = \kappa_e \arctan \frac{\bar{z}_i - \bar{z}_{i+1}}{l_{i,i+1}} \tag{5}$$

$$f = \kappa_f \frac{\sum_{j=1}^{N} \left(e^z \cdot x^j\right)^4}{N} \tag{6}$$

$$\lambda = \begin{cases} 1 & r > r_{\max} \\ \frac{r - r_{\min}}{r_{\max} - r_{\min}} & r \in [r_{\min}, r_{\max}] \wedge |\Sigma|_F^2 < t_{\text{trace}} \\ 0 & \text{otherwise} \end{cases} \tag{7}$$

where κ_s, κ_e, κ_f are constant coefficients. e^z represents the unit normal vector of the fitted plane. $\bar{z}_{e^z}$ signifies the projection of the plane normal vector on the Z-axis of the world coordinate system. $l_{i,i+1}$ represents the horizontal distance between $\mathcal{N}_i$ and $\mathcal{N}_{i+1}$. The variable r denotes the proportion of vacant space in the plane, and once it surpasses the predefined threshold for vacant space ratio, it suggests the presence of depressions in the ground. Moreover, to maintain the smoothness of the fitted plane, the expansion distance of PA-RRT* must ensure that the step size $l_{i,i+1}$ satisfies $l_{i,i+1} < l_{cube}/2$. As shown in Fig. 2 (bottom right), flat areas have a cost close to 0, gentle slopes around 0.3, and steep slopes almost 1 resulting in their exclusion from the traversable areas. Likewise, the nodes located within hollows are also excluded from consideration.

2) PA-RRT Generation:*

The generation of the local exploration path in this paper is based on PA-RRT*, as detailed in Algorithm 1. Firstly, a local tree denoted as $\mathbb{T}_L$, which includes the vertex set $\mathbb{V}$ and edge set $\mathbb{E}$, is incrementally constructed within the subset $\mathcal{M}_{sub}$. $\mathbb{T}_L$ starts from the current state of the robot ψ_c. During each iteration, a space point $\mathbf{x}_{rand}$ is randomly generated within the region $\mathcal{M}_{sub}$. This point is projected onto the surface, which yields a surface point denoted as $\tilde{\mathbf{x}}_{rand}$. The planner then finds its closet point $\tilde{\mathbf{x}}_{near}$ in $\mathbb{T}_L$. After that, our method verifies if the distance between $\tilde{\mathbf{x}}_{near}$ and $\tilde{\mathbf{x}}_{rand}$ is less than half of l_{cube}. If this condition is met, $\tilde{\mathbf{x}}_{rand}$ is directly chosen as $\tilde{\mathbf{x}}_{new}$. Otherwise, a new sampling point $\mathbf{x}_{new}$ is generated by extending a distance of $l_{cube}/2$ from $\tilde{\mathbf{x}}_{near}$ to $\tilde{\mathbf{x}}_{rand}$ and then projecting it to obtain $\tilde{\mathbf{x}}_{new}$. Next, the terrain cost $\mathcal{F}(\mathcal{N}_{new}, \mathcal{N}_{near})$ is computed based on the corresponding planes of the two nodes. Any sampling points exceeding the predefined threshold value of $\mathcal{F}(\mathcal{N}_{new}, \mathcal{N}_{near})$ are discarded.

In complex environments with uneven surfaces, verifying the collision detection between the new node $\mathcal{N}_{new}$ and its nearest node $\mathcal{N}_{near}$ is insufficient. To avoid potential collisions and ensure the stability and smooth operation of the system, it is crucial to evaluate whether the new node falls within the traversable space $\mathcal{X}_{trav}$ and discard nodes that exceed Δe_{max}. If the above conditions are satisfied, a set of neighboring nodes $\Xi_{neighbor}$ within a specified range is examined. If the terrain cost $\mathcal{F}(\mathcal{N}_{new}, \mathcal{N}_{parent})$ is less than $\mathcal{F}(\mathcal{N}_{new}, \mathcal{N}_{near})$, $\mathcal{N}_{parent}$ is selected as the parent node for the pruning operation. The process of constructing a local tree $\mathbb{T}_L$ by adding vertices and edges is continued until it reaches a predefined maximum limit of vertices $N_{\mathbb{V},max}$ or edges $N_{\mathbb{E},max}$. By iterating the above process, a sequence of nodes $\{\mathcal{N}_i\}$ is obtained that facilitates ground robots movement, which is equivalent to receiving a serial of planes $\{P_i\}$ that are connected to form a strip area, as illustrated in Fig. 3. This strip area provides accurate terrain assessment for Section III-C.

C. Dual-Layer Exploration Framework

1) Local Planner:

In response to the need for safe exploration in complex and sub-paths rugged environments, the local planner ensures that the robot adopts an efficient exploratory strategy tailored to uneven terrain by utilizing PA-RRT*. As detailed in Algorithm 1, given a local tree $\mathbb{T}_L = (\mathbb{V}, \mathbb{E})$ constructed by PA-RRT*, Dijkstra [28] is employed to find the set of shortest paths $\Sigma_{\sigma,L}$ from the root vertex ψ_c to all remaining vertices within the vertices set $\mathbb{V}$, which aims to enhance exploration efficiency. The generation of the local exploration path is based on each node in $\mathbb{T}_L$, which employs Truncated Signed Distance Fields (TSDFs) [29] to appraise the exploration gain. The TSDF map classifies grid states as Unknown, Free, or Occupied, which provides details on space occupancy and distance to the nearest surface. Then, the planner calculates the volumetric gain $\mathbf{VG}$ for each vertex in $\mathbb{V}$, which utilizes a sensor ray model to analyze the number of voxels in the TSDF map intersected by rays emitted from nodes. Through the assignment of weight to different voxel states, nodes with more unknown states receive higher volumetric gain, which enables efficient path selection for exploring unknown regions with minimal computational burden. Considering the distribution of terrain cost, our method optimizes the local path to adeptly traverse diverse terrain types while prioritizing the safety and stability of the robot. This holistic assessment of terrain cost and $\mathbf{VG}$ for nodes augments the reliability of the exploration framework in challenging environments. Considering terrain cost, volumetric gain, and other functions related to distance and direction are taken into account for the calculation of the exploration gain related to each shortest path in $\sigma_i \in \Sigma_{\sigma,L}, i = 1, 2, \ldots, n$ with a set of vertices along the path $\mathcal{N}_j^i \in \sigma_i, j = 1, 2, \ldots, m_i$, the local exploration gain $\mathcal{E}_L(\sigma_i)$ is calculated as follows:

$$\mathcal{E}_L(\sigma_i) = e^{-\gamma_S \mathcal{S}(\sigma_i, \sigma_{exp})} \sum_{j=1}^{m_i} \mathbf{VG}\left(\mathcal{N}_j^i\right) e^{-\gamma_D \mathcal{D}\left(\mathcal{N}_1^i, \mathcal{N}_j^i\right)} e^{-\gamma_F \mathcal{F}\left(\mathcal{N}_j^i, \mathcal{N}_{j-1}^i\right)} \tag{8}$$

where $\mathcal{S}(\sigma_i, \sigma_{exp})$, $\mathcal{D}\left(\mathcal{N}_1^i, \mathcal{N}_j^i\right)$, and $\mathcal{F}(\mathcal{N}_j^i, \mathcal{N}_{j-1}^i)$ represent cost functions for path orientation, distance, and terrain, respectively. γ_S, γ_D, and γ_F are the adjustable weight. $\mathcal{D}\left(\mathcal{N}_1^i, \mathcal{N}_j^i\right)$ represents the cumulative Euclidean distance from the root node of the exploration tree to each node $\mathcal{N}_j^i$ along the path σ_i, which prioritizes paths with a higher volume gain to distance ratio. $\mathcal{S}(\sigma_i, \sigma_{\text{exp}})$ compares the similarity between the planned path σ_i and a pseudo straight path σ_{exp} of equal length in the estimated exploration direction, which prioritizes exploration in the same direction as the preceding path. The local planner iterates until the global planner is triggered or until a predefined maximum number of sampling nodes in $\mathbb{T}_L$ is attained. Ultimately, exploration gains for all paths are calculated, resulting in a set $\Sigma_{E(\sigma_L)}$ from which the path with the highest gain $\sigma_{L,\,best}$ is selected as the optimal path for execution.

2) Global Planner:

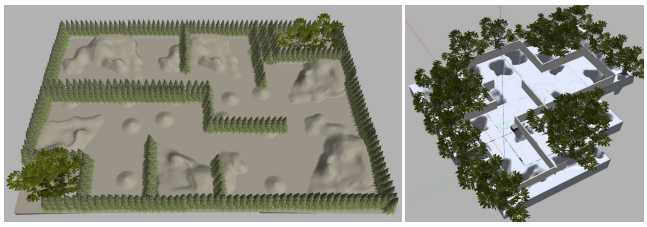

(a) (b)

Fig. 4. The two simulation environments: (a) The hills scenario. (b) The hollows scenario.

(a) (b)

Fig. 5. The vehicle platform used for our experiments, Bulldog, is equipped with OS1-32-U LiDAR and a Wi-Fi Module for communication. It is shown: (a) The main view. (b) The side view.

The global planner ensures exploration capability by searching for alternative paths to unexplored areas in the case of local planning failure and managing the homing process when time constraint is reached. We propose a method that involves incrementally constructing and maintaining a graph based on the local tree $\mathbb{T}_L$. It also considers paths with high exploration gain to maintain a selective list of potential vertices indicating unexplored regions. This list periodically updates to accommodate changes in exploration gain. After local exploration, the Dijkstra is used to ascertain the shortest path $\sigma_{G,\,i}$ to all boundary nodes in the global graph, while computing exploration gain values for each path. The global exploration gain $\mathcal{E}_G\left(\sigma_{G,i}\right)$ is calculated as follows:

$$\mathcal{E}_G\left(\sigma_{G,i}\right) = \mathbf{VG}\left(\mathcal{N}_{G,i}\right) e^{-\mu_D \mathcal{D}\left(\mathcal{N}_{cur}, \mathcal{N}_{G,i}\right)} e^{-\mu_F \mathcal{F}\left(\mathcal{N}_{cur}, \mathcal{N}_{G,i}\right)} \tag{9}$$

where $\mathbf{VG}\left(\mathcal{N}_{G,i}\right)$ denotes the volumetric gain of the current boundary node. $\mathcal{D}\left(\mathcal{N}_{cur}, \mathcal{N}_{G,i}\right)$ and $\mathcal{F}\left(\mathcal{N}_{cur}, \mathcal{N}_{G,i}\right)$ represent the cost function of the distance and terrain, respectively, from the current node to the global exploration boundary node. μ_D and μ_F are the adjustable weight. $\mathcal{D}\left(\mathcal{N}_{cur}, \mathcal{N}_{G,i}\right)$ penalizes excessive distance, while $\mathcal{F}\left(\mathcal{N}_{cur}, \mathcal{N}_{G,i}\right)$ penalizes paths with higher terrain cost. This prioritizes the exploration of nearby boundary nodes and encourages the generation of paths with lower terrain cost. As exploration progresses, the TSDF map is continuously updated, potentially leading to diminished or eliminated volumetric gains $\mathbf{VG}\left(\mathcal{N}_{G,i}\right)$ for boundary nodes. Once the completion of boundary exploration or reaching a predefined coverage ratio $\mathcal{V}_{exp}/\mathcal{V}$ is reached, the global planner restarts. Then, a path is calculated from the current location back to the initial node.

IV. Experiments

To fully evaluate the efficiency and robustness of our proposed method, we conducted a series of quantitative and qualitative experiments in both benchmark and real-world scenarios. The real-world experiments utilized the Bulldog, a

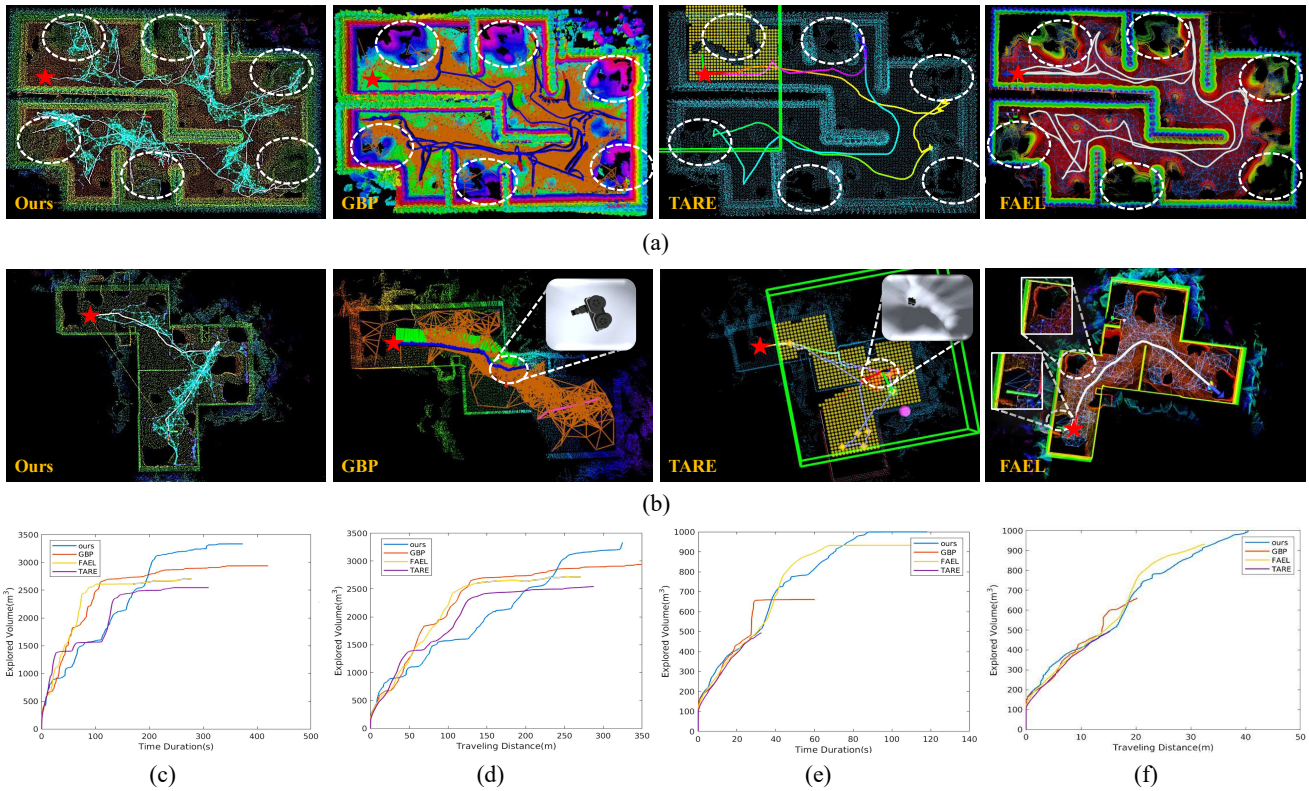

Fig. 6. A benchmark comparison was conducted among our proposed method, GBP, TARE, and FAEL as depicted in Fig. 4(a) and Fig. 4(b). The red star denotes the initial point of exploration. (a) illustrates the experimental results in the hilly environment, highlighting the area overlooked by all methods except ours with white dotted circles. (c) and (d) portray changes in exploration volume and distance traveled over time for the four methods in the hilly environment. (b) displays the results of the hollows environment, where UGV encounters challenges with GBP and TARE and is unable to complete the subsequent exploration, while FAEL generates a roadmap for hazardous hollows, as shown in the zoomed-in section. (e) and (f) also demonstrate changes in exploration volume and distance traveled over time for the four methods in the hollow environment.

four-wheel differential mobile robot, as depicted in Fig. 5. It is equipped with an Ouster LiDAR OS1-32-U and an Xsens XTI-300, together with an onboard computer (i7-9600k CPU and 16 GB RAM). A SLAM module adopting Fast-lio [30] is utilized for the localization of the Bulldog.

A. Simulation Experiments

Our proposed method was evaluated in a simulated terrain with hills and hollows, comparing it with GBP [24], TARE [8], and FAEL [27] under the identical conditions across four key metrics: run time, exploration volume, traveling distance, and exploration time. Utilizing a global TSDF map at 0.2m resolution and a local 3D grid map at 0.1m resolution, the PA-RRT* planar evaluation conducts random sampling in a $20m \times 20m \times 3m$ cube around the robot center. The maximum velocity of the robot is $v_{\max} = 1.5m/s$, with exploration ending when 95% of the specified area was covered. Each method is run 20 times initiating from the same starting position and executed for 10 min per simulated exploration in both scenarios. The results and exploration details are summarized in Tab. I, with exploration volume efficiency shown in Tab. II. Here, the variable ξ is defined as the exploration volume resulting from the completion of the algorithm's execution, and the relative efficiency ratio r_ξ indicates the explored volume ratio of the comparative methods to our approach.

1) Hills Scenario:

In a simulated scenario spanning a $42 \times 40m^2$ area with hills, as illustrated in Fig. 4(a), we conducted a comprehensive comparison of four methods. The results reveal the superior performance of our proposed method, particularly in achieving an exceptional exploration volume, which is attributed to its planar assessment that guides paths adhering to traversability constraints. This achievement is emphasized by the dashed circles in Fig. 6(a). In contrast, other methods, lacking comprehensive traversability assessment, struggled to secure viable exploration paths or failed to meet volume thresholds. The curves depicting the explored volume, varying with time duration and traveling distance for each method, are illustrated in Fig. 6(c) and Fig. 6(d). Notably, our proposed approach employs PA-RRT* with terrain analysis to generate exploration paths that traverse from flat ground to gentle slop. Conversely, our method obtains exploration volumes overlooked by other methods, which usually provide only rudimentary assessments of traversable areas and fail to identify paths to the mountains. Our approach achieves an impressive average exploration volume of $3334m^3$ and covers the distance in a period of $262.6s$, showcasing a $721m^3$ higher volume compared to FAEL. To mitigate the risk of UGV rollover, our method adeptly navigates suitable terrain and travels to and from rugged areas, resulting in increased traveling distance and exploration time. Despite its

TABLE I

RESULTS OF SIMULATIONS IN HILLS AND HOLLOWS SCENARIOS

Scene	Method	Run Time(s)	Exploration Volume(m^3)		Traveling distance(m)		Exploration Time(s)	
			Avg	Std	Avg	Std	Avg	Std
Hills	GBP [24]	0.892	2938	286	342.3	51.2	350.0	49.2
	TARE [8]	0.618	2545	127	287.1	34.9	252.8	32.0
	FAEL [27]	**0.297**	2613	103	**273.7**	29.7	**247.4**	**18.1**
	Ours	0.323	**3334**	**78**	324.0	**24.4**	262.6	28.2
Hollows	GBP [24]	0.55	>529	–	>20	–	>34.5	–
	TARE [8]	0.23	>494	–	>15.2	–	>32.7	–
	FAEL [27]	**0.18**	932	34	**32.6**	5.8	**68.5**	**4.9**
	Ours	0.21	**998**	**27**	40.1	**3.7**	81.2	6.3

* '–' represents the method that has failed.

TABLE II

COMPARISON OF EXPLORATION VOLUME EFFICIENCY

Scene	GBP		TARE		FAEL		Ours	
	ξ	r_ξ	ξ	r_ξ	ξ	r_ξ	ξ	r_ξ
Hills	2938	0.88	2545	0.76	2613	0.78	**3334**	**1.0**
Hollows	529	0.53	494	0.49	932	0.93	**998**	**1.0**

sub-optimal runtime, the algorithm meets real-time demands, leading to increased exploration volume and adaptability to varied terrain, which leads to a notable boost in exploration volume and adaptability to diverse terrain. Our method demonstrates a remarkable efficiency increase of over 12% on average in exploration volume compared to other methods, as illustrated in Table II.

2) Hollows Scenario:

In a scenario featuring hollows, with a region measuring $30 \times 35m^2$ depicted in Fig. 4(b), we conducted a comprehensive comparison of four exploration methods. Both GBP and TARE faced challenges to fully explore the environment within the allocated time limits, as shown in Fig. 6(b). On the other hand, FAEL utilized information gain based on the ground point cloud to accomplish exploration. Notably, Fig. 6(b) displays the road map generated by FAEL within the region outlined by the white dashed circles, which poses a potential risk of the UGV falling into hollows. In contrast, we implemented a proactive strategy by setting high traversal costs for the hollows and their surrounding environments using the terrain analysis module proposed earlier. This strategy prevented the generation of paths within hollow environments during PA-RRT*, ensuring safe motion. The results of the four methods regarding exploration volume over time duration and traveling distance are illustrated in Fig. 6(e) and Fig. 6(f). Additionally, Tab. II provides a comprehensive overview of the exploration volume efficiency for each method. The results highlight the effectiveness of our proposed strategy in addressing challenges posed by hollow terrain, ensuring safer and more efficient autonomous exploration.

B. Real-World Experiment

To further validate our proposed approach, we conducted extensive real-world experiments in unknown and uneven terrain. The first scenario involved a flat bridge, as shown in Fig. 7, where the Bulldog simultaneously mapped an

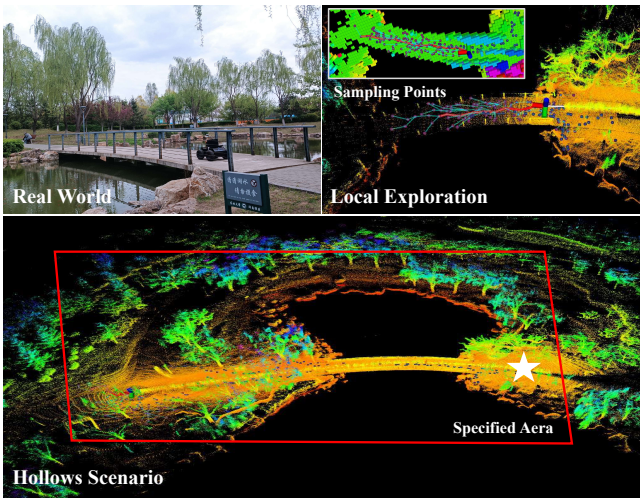

Fig. 7. Instances of autonomous plane-assisted exploration path planning in hollows experiments. The white star marks the starting point, the red square represents specified areas, and the white line represents the exploration path followed. The results showed that sampling points were only generated within the flat bridge and did not extend beyond it, confirming the robust navigation capabilities of PARE.

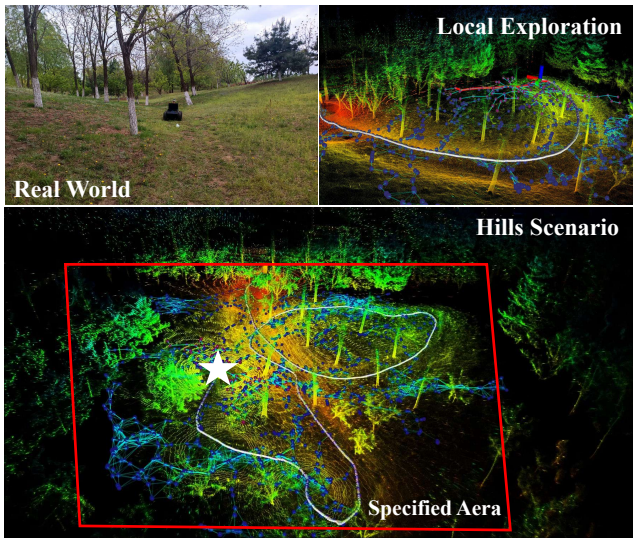

Fig. 8. An exploration experiment conducted in a forest with hills terrain. The upper side of the figure shows the actual environment and local exploration tree renderings, while the bottom side displays the results of the environmental exploration. The white star marks the starting point, and the white line represents the exploration path followed.

unknown space and navigated around obstacles. The exploration area spans $50 \times 170m^2$, with Bulldog covering a distance of $134m$ and completing the task in $173s$. The surroundings of the flat bridge are primarily composed of expansive water surface and the bridge deck. In this particular setting, it is crucial for our method to avoid generating any exploration paths that traverse the water surface. Given the notable difference in elevation between the water surface and the bridge deck, our approach strategically filters out nodes, which allows only those positioned on the bridge deck to successfully navigate through the discerning process of the terrain evaluation module. Through this filtering mechanism, we ensure that the robot only generates paths on the bridge

deck, rather than the surrounding water surface. The second scenario featured a hilly area with varying slopes, as depicted in Fig. 8, where the white line represents the trajectory of the robot and the blue dots mark the global graph. The size of the exploration area is about $110 \times 170m^2$, and the Bulldog traveled a distance of $192m$ within $230s$ to complete the exploration. The results indicate that our method is well-suited for accomplishing autonomous exploration in unknown and uneven terrain. More details can be available at $https://youtu.be/v_T0OY1Riks$.

V. CONCLUSIONS

We propose a novel dual-layer exploration framework named PARE, designed to address the challenges posed by traversable obstacles in uneven terrain while enhancing exploration capabilities in unknown and rugged regions. Our approach utilizes PA-RRT* to construct a local exploration tree, evaluating traversability to ensure secure access to the target area. Then, we implement a dual-layer exploration framework, integrating both local and global strategies to achieve a significantly larger exploration volume. Experimental results demonstrate the superiority of our method in scenarios featuring hills and hollows, achieving increased exploration volume by over 12% on average compared to the existing framework. In the future, we aim to showcase the algorithm's performance in a real environment with deformable terrain.

REFERENCES

[1] S. Omari, P. Gohl, M. Burri, M. Achtelik, and R. Siegwart, "Visual industrial inspection using aerial robots," in *Proceedings of the 2014 3rd International Conference on Applied Robotics for the Power Industry*, pp. 1–5, IEEE, 2014.

[2] T. Dang, C. Papachristos, and K. Alexis, "Autonomous exploration and simultaneous object search using aerial robots," in *2018 IEEE Aerospace Conference*, pp. 1–7, IEEE, 2018.

[3] L. Schmid, M. Pantic, R. Khanna, L. Ott, R. Siegwart, and J. Nieto, "An efficient sampling-based method for online informative path planning in unknown environments," *IEEE Robotics and Automation Letters*, vol. 5, no. 2, pp. 1500–1507, 2020.

[4] Z. Jia, W. Smith, and H. Peng, "Terramechanics-based wheel–terrain interaction model and its applications to off-road wheeled mobile robots," *Robotica*, vol. 30, no. 3, pp. 491–503, 2012.

[5] J. Billingsley, A. Visala, and M. Dunn, "Robotics in agriculture and forestry," 2008.

[6] F. Bourgault, A. A. Makarenko, S. B. Williams, B. Grocholsky, and H. F. Durrant-Whyte, "Information based adaptive robotic exploration," in *IEEE/RSJ international conference on intelligent robots and systems*, vol. 1, pp. 540–545, IEEE, 2002.

[7] H. Zhu, C. Cao, Y. Xia, S. Scherer, J. Zhang, and W. Wang, "Dsvp: Dual-stage viewpoint planner for rapid exploration by dynamic expansion," in *2021 IEEE/RSJ International Conference on Intelligent Robots and Systems (IROS)*, pp. 7623–7630, IEEE, 2021.

[8] C. Cao, H. Zhu, H. Choset, and J. Zhang, "Tare: A hierarchical framework for efficiently exploring complex 3d environments.," in *Robotics: Science and Systems*, vol. 5, 2021.

[9] P. Fankhauser, M. Bloesch, and M. Hutter, "Probabilistic terrain mapping for mobile robots with uncertain localization," *IEEE Robotics and Automation Letters*, vol. 3, no. 4, pp. 3019–3026, 2018.

[10] M. Mattamala, N. Chebrolu, and M. Fallon, "An efficient locally reactive controller for safe navigation in visual teach and repeat missions," *IEEE Robotics and Automation Letters*, vol. 7, no. 2, pp. 2353–2360, 2022.

[11] E. Stumm, A. Breitenmoser, F. Pomerleau, C. Pradalier, and R. Siegwart, "Tensor-voting-based navigation for robotic inspection of 3d surfaces using lidar point clouds," *The International Journal of Robotics Research*, vol. 31, no. 12, pp. 1465–1488, 2012.

[12] S. Garrido, M. Malfaz, and D. Blanco, "Application of the fast marching method for outdoor motion planning in robotics," *Robotics and Autonomous Systems*, vol. 61, no. 2, pp. 106–114, 2013.

[13] P. Krüsi, P. Furgale, M. Bosse, and R. Siegwart, "Driving on point clouds: Motion planning, trajectory optimization, and terrain assessment in generic nonplanar environments," *Journal of Field Robotics*, vol. 34, no. 5, pp. 940–984, 2017.

[14] F. S. Barbosa, D. Duberg, P. Jensfelt, and J. Tumova, "Guiding autonomous exploration with signal temporal logic," vol. 4, pp. 3332–3339, IEEE, 2019.

[15] Z. Jian, Z. Lu, X. Zhou, B. Lan, A. Xiao, X. Wang, and B. Liang, "Putn: A plane-fitting based uneven terrain navigation framework," in *2022 IEEE/RSJ International Conference on Intelligent Robots and Systems (IROS)*, pp. 7160–7166, 2022.

[16] B. Yamauchi, "A frontier-based approach for autonomous exploration," in *Proceedings 1997 IEEE International Symposium on Computational Intelligence in Robotics and Automation CIRA'97.'Towards New Computational Principles for Robotics and Automation'*, pp. 146–151, IEEE, 1997.

[17] A. Dai, S. Papatheodorou, N. Funk, D. Tzoumanikas, and S. Leutenegger, "Fast frontier-based information-driven autonomous exploration with an mav," in *2020 IEEE international conference on robotics and automation (ICRA)*, pp. 9570–9576, IEEE, 2020.

[18] H. H. González-Banos and J.-C. Latombe, "Navigation strategies for exploring indoor environments," *The International Journal of Robotics Research*, vol. 21, no. 10-11, pp. 829–848, 2002.

[19] T. Cieslewski, E. Kaufmann, and D. Scaramuzza, "Rapid exploration with multi-rotors: A frontier selection method for high speed flight," in *2017 IEEE/RSJ International Conference on Intelligent Robots and Systems (IROS)*, pp. 2135–2142, IEEE, 2017.

[20] C. Witting, M. Fehr, R. Bähnemann, H. Oleynikova, and R. Siegwart, "History-aware autonomous exploration in confined environments using mavs," in *2018 IEEE/RSJ International Conference on Intelligent Robots and Systems (IROS)*, pp. 1–9, IEEE, 2018.

[21] A. Bircher, M. Kamel, K. Alexis, H. Oleynikova, and R. Siegwart, "Receding horizon path planning for 3d exploration and surface inspection," *Autonomous Robots*, vol. 42, pp. 291–306, 2018.

[22] C. Papachristos, S. Khattak, and K. Alexis, "Uncertainty-aware receding horizon exploration and mapping using aerial robots," in *2017 IEEE international conference on robotics and automation (ICRA)*, pp. 4568–4575, IEEE, 2017.

[23] T. Dang, C. Papachristos, and K. Alexis, "Visual saliency-aware receding horizon autonomous exploration with application to aerial robotics," in *2018 IEEE International Conference on Robotics and Automation (ICRA)*, pp. 2526–2533, IEEE, 2018.

[24] T. Dang, M. Tranzatto, S. Khattak, F. Mascarich, K. Alexis, and M. Hutter, "Graph-based subterranean exploration path planning using aerial and legged robots," *Journal of Field Robotics*, vol. 37, no. 8, pp. 1363–1388, 2020.

[25] M. Selin, M. Tiger, D. Duberg, F. Heintz, and P. Jensfelt, "Efficient autonomous exploration planning of large-scale 3-d environments," *IEEE Robotics and Automation Letters*, vol. 4, no. 2, pp. 1699–1706, 2019.

[26] M. Dharmadhikari, T. Dang, L. Solanka, J. Loje, H. Nguyen, N. Khedekar, and K. Alexis, "Motion primitives-based path planning for fast and agile exploration using aerial robots," in *2020 IEEE International Conference on Robotics and Automation (ICRA)*, pp. 179–185, IEEE, 2020.

[27] J. Huang, B. Zhou, Z. Fan, Y. Zhu, Y. Jie, L. Li, and H. Cheng, "Fael: Fast autonomous exploration for large-scale environments with a mobile robot," *IEEE Robotics and Automation Letters*, 2023.

[28] T. H. Cormen, C. Leiserson, R. Rivest, and C. Stein, "Introduction to algorithms, book," 2009.

[29] D. Werner, A. Al-Hamadi, and P. Werner, "Truncated signed distance function: experiments on voxel size," in *Image Analysis and Recognition: 11th International Conference, ICIAR 2014, Vilamoura, Portugal, October 22-24, 2014, Proceedings, Part II 11*, pp. 357–364, Springer, 2014.

[30] W. Xu and F. Zhang, "Fast-lio: A fast, robust lidar-inertial odometry package by tightly-coupled iterated kalman filter," *IEEE Robotics and Automation Letters*, vol. 6, no. 2, pp. 3317–3324, 2021.